RADIO SCIENCE, VOL. 46, RS4006, doi:10.1029/2010RS004530, 2011

Broadband and low-beam squint leaky wave radiation from a uniaxially anisotropic grounded slab

A. Shahvarpour,[1] C. Caloz,[1] and A. Alvarez-Melcon[2]

Received 21 September 2010; revised 27 January 2011; accepted 29 April 2011; published 4 August 2011.

[1] The behavior of leaky and surface modes in uniaxially anisotropic grounded slabs is investigated. First, a transverse magnetic and transverse electric modal parametric analysis of the structure is performed, based on dispersion relations, comparing the nondispersive and Drude/Lorentz dispersive anisotropic slabs with an isotropic nondispersive slab. This analysis reveals that in the case of the isotropic slab, the leaky wave pointing angle is restricted to the end-fire region. In contrast, it is shown, for the first time, that the proposed anisotropic dispersive grounded slab structure provides efficient (in particular highly directive) leaky wave radiation with a high design flexibility. Toward its lower frequencies, the dominant leaky mode provides full-space conical-beam scanning. At higher frequencies, it provides fixed-beam radiation (at a designable angle) with very low beam squint. A vertical dipole source is placed inside the slab to excite the relevant leaky wave mode. The radiation characteristics obtained for this structure confirms the novel low-beam squint and high-directivity operation of the dominant leaky mode. Further validation is included using the commercial software tool CST. The structure could be used to conceive antennas either for conical beam scanning (lower-frequency range) or for point-to-point communication and radar systems (higher-frequency range).

Citation: Shahvarpour, A., C. Caloz, and A. Alvarez-Melcon (2011), Broadband and low-beam squint leaky wave radiation from a uniaxially anisotropic grounded slab, *Radio Sci.*, *46*, RS4006, doi:10.1029/2010RS004530.

1. Introduction

[2] Leaky wave antennas feature high directivity and frequency beam scanning capability. They have found many applications in radar, point-to-point communications and MIMO systems. The general theory of leaky wave antennas and the history of their developments have been reported by *Oliner and Jackson* [2007]. Slitted waveguide [see *Hansen*, 1940], holey waveguide [see *Hines and Upson*, 1957] and sandwiched line [see *Rotman and Karas*, 1957] antennas were the first proposed fan beam leaky wave antennas, while high-directivity leaky wave antenna constituted by periodic partially reflective screens over a ground plane [see *Trentini*, 1956], or dielectric superstrate layers [see *Jackson and Oliner*, 1988] and several other types performed by various authors [see *Ip and Jackson*, 1990; *Jackson et al.*, 1993; *Feresidis and Vardaxoglou*, 2001; *Zhao et al.*, 2005], enabled the conical-beam radiation.

[3] Over the past decade, intense research has been performed in the area of electromagnetic metamaterials [see *Caloz and Itoh*, 2006; *Engheta and Ziolkowski*, 2006; *Capolino*, 2009]. In the microwave range, transmission line type metamaterials have led to a wealth of component [see *Lai et al.*, 2004; *Eleftheriades*, 2007], antenna [see *Caloz et al.*, 2008] and system [see *Gupta and Caloz*, 2009] applications. However, most of the planar metamaterial structures were in fact structured transmission lines printed on conventional standard substrate and thus were not "real" metamaterials but rather artificial transmission lines with periodic loads. However, real *metasubstrates*, or artificial dielectric substrates, have recently been introduced [see *Ikonen et al.*, 2006; *Mosallaei and Sarabandi*, 2007; *Nguyen and Caloz*, 2007; *Coulombe et al.*, 2007]. Also, several leaky wave antennas based on metasubstrates have been reported in the past [see *Allen et al.*, 2004, 2005; *Lovat et al.*, 2006; *Burghignoli et al.*, 2008]. However, some of the previous works [see *Allen et al.*, 2004, 2005] treated the antenna design problem from an experimental perspective, and detailed in-depth studies on the properties and behavior of these new metasubstrates are lacking.

[4] To fill the above gap, this paper presents a detailed investigation of the leaky and surface modes that can propagate in a uniaxially permittivity and permeability anisotropic grounded slab using a spectral domain approach based on transmission line equivalent circuits. The structure is assumed to behave with a Drude dispersive permittivity along the axis perpendicular to the substrate and with a Lorentz permeability in the plane of the substrate. Such a substrate may be implemented in the form of a mushroom-type structure [see *Sievenpiper et al.*, 1999; *Nguyen and Caloz*, 2007; *Yakovlev et al.*, 2009], where the Drude

[1]Poly Grames Research Center, Department of Electrical Engineering, École Polytechnique de Montréal, Centre de Recherche en Électronique Radiofréquence, Montréal, Quebec, Canada.
[2]Department of Information and Communication Technologies, Technical University of Cartagena, Cartagena, Spain.

0048-6604/11/2010RS004530

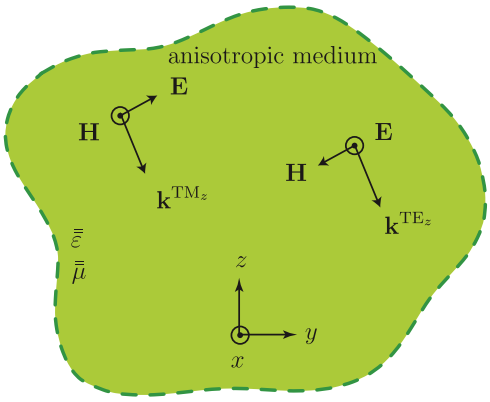

Figure 1. Effective uniaxial anisotropic medium (unbounded), characterized by the permittivity and permeability tensors of equation (1) along with the TM_z and TE_z field configurations.

dispersive permittivity models the wires and the Lorentz dispersive permeability models the rings between adjacent mushrooms in the plane of the substrate. The complete structure includes two distinct dispersion levels, whose combination leads to the overall structure's dispersion. The first level refers to the dispersive behavior of the grounded slab itself, even present in the case where the slab is isotropic. The second level refers to the Drude and Lorentz model of the artificial materials constituting the slab. It is shown, for the first time, that such a structure can propagate a leaky wave mode which can support broadband, highly directive and low-beam squint radiation in the upper part of the right-handed (RH) region, in contrast to isotropic structures (conventional grounded dielectric slabs). It is also shown that this novel low-beam squint effect cannot be achieved using simple ferrite type materials, even if they also exhibit Lorentz type dispersive permeability response.

[5] A vertical source is introduced in the slab to excite the dominant leaky mode. By computing the radiation characteristics of this structure the novel low-beam squint and high-directivity characteristics of the mode are confirmed. The behavior is further verified using the CST commercial software tool.

[6] The paper first investigates the transverse magnetic (TM) and transverse electric (TE) dispersion properties of the uniaxially anisotropic grounded slab. Section 4 presents a modal parametric analysis, comparing the nondispersive and Drude/Lorentz dispersive anisotropic slabs with the isotropic nondispersive slab. As the TM modes are found in this section more appropriate for broadband, low-beam squint leaky wave radiation, section 5 employs a vertical point source for the excitation of the TM leaky modes. Then, the asymptotic far-field radiation properties are computed from the Green's functions using the transmission line model of the structure [see *Mosig*, 1989]. Finally, in section 6 the radiation properties of the isotropic and anisotropic slabs are carefully compared.

2. Definition of the Medium

[7] The uniaxially anisotropic medium of interest is represented in Figure 1 along with the TM_z and TE_z field configurations, where z will be the axis perpendicular to the air-dielectric interface in the grounded anisotropic slab which will be studied in section 3. The medium is characterized by the following permittivity and permeability tensors

$$\bar{\bar{\varepsilon}} = \begin{pmatrix} \varepsilon_\rho & 0 & 0 \\ 0 & \varepsilon_\rho & 0 \\ 0 & 0 & \varepsilon_z \end{pmatrix}, \tag{1a}$$

$$\bar{\bar{\mu}} = \begin{pmatrix} \mu_\rho & 0 & 0 \\ 0 & \mu_\rho & 0 \\ 0 & 0 & \mu_z \end{pmatrix}. \tag{1b}$$

For typical artificial substrates, such as mushroom-type structures [see *Sievenpiper et al.*, 1999], ε_z and μ_ρ may represent the permittivity and permeability, respectively, due to the presence of the artificial implants, while ε_ρ and μ_z represent the permittivity and permeability, respectively, of a host medium (e.g., Teflon) [see *Nguyen and Caloz*, 2007].

[8] While the host medium is generally nondispersive, the constitutive parameters related to the artificial implants are inherently dispersive (i.e., frequency-dependent). In the frequency range where the wires of the mushroom-type structure are electrically short or densely packed [see *Yakovlev et al.*, 2009], the effective permittivity term ε_z may be modeled by the electric local Drude dispersion expression [see *Tretyakov*, 2003]

$$\frac{\varepsilon_z}{\varepsilon_0} = \varepsilon_r \left[1 - \frac{\omega_{pe}^2}{\omega^2 - j\omega\zeta_e} \right], \tag{2}$$

where ε_r is the host medium permittivity, ω_{pe} is the electric plasma frequency, which is related to the lattice constant and ζ_e is the damping factor of the structure. Moreover, the effective permeability term μ_ρ may be modeled by the magnetic Lorentz dispersion relation [see *Pendry et al.*, 1999]

$$\begin{aligned} \frac{\mu_\rho}{\mu_0} &= 1 - \frac{F\omega^2}{(\omega^2 - \omega_{m0}^2) - j\omega\zeta_m} \\ &= 1 - \frac{F\omega^2}{\left[\omega^2 - \omega_{pm}^2(1-F)\right] - j\omega\zeta_m}, \end{aligned} \tag{3}$$

where F is a factor related to the geometry of the current loops, ω_{m0} is the resonant frequency of these loops, $\omega_{pm} = \omega_{m0}/\sqrt{1-F}$ is the plasma frequency and ζ_m is the damping factor of the structure.

[9] Following *Nguyen and Caloz* [2007], we assume that the uniaxially anisotropic grounded slab exhibits the dispersive responses of equations (2) and (3) in the frequency range of interest. However, at higher frequencies, where the electrical thickness of the substrate becomes relatively large, the permittivity dispersion of equation (2) would have to be modified to follow a nonlocal model to take into account spatial dispersion [see *Yakovlev et al.*, 2009]. Moreover, as the frequency increases far above the electric and magnetic plasma frequencies, ω_{pe} and ω_{pm}, respectively, the artificial mushroom structure progressively looses its homogeneity, since the electrical size of the unit cell grows, and therefore the effective anisotropic medium models of equations (1) with the effective dispersive permittivity and permeability of equations (2) and (3), respectively, eventually become

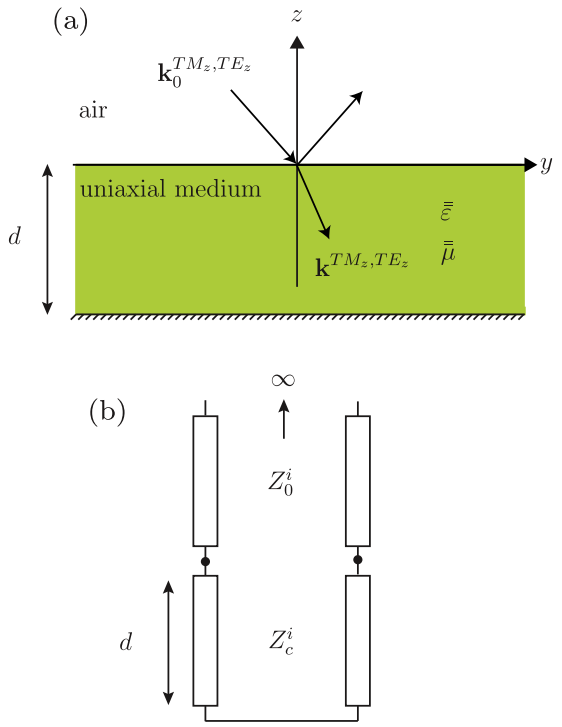

Figure 2. Uniaxially anisotropic grounded slab and its transmission line model, where $i \equiv TM_z, TE_z$. (a) TM_z and TE_z waves incident onto the slab. (b) Transmission line model (sourceless case).

inappropriate. However, in the following theoretical study, it is assumed that the medium remains effectively Drude/Lorentz dispersive in a wideband frequency range, as allowed by some unit-cell compression techniques, such as for instance the use of elongated mushroom structures [see *Coulombe et al.*, 2010] or of nanostructured metamaterials [see *Carignan et al.*, 2011]. Such techniques may be used in the future practical implementation of the wideband anisotropic materials.

3. Dispersion Relation of the Uniaxially Anisotropic Grounded Slab

[10] Figure 2a shows the grounded uniaxial anisotropic slab of interest. The TM_z and TE_z dispersion relations for this structure are derived by the transverse resonance technique [see *Marcuvitz*, 1951] with the help of the sourceless transmission line model [see *Felsen and Marcuvitz*, 1996] shown in Figure 2b. They read

$$jZ_c^{TM_z,TE_z}\tan\left(\beta_z^{TM_z,TE_z}d\right) + Z_{c0}^{TM_z,TE_z} = 0, \tag{4}$$

where $\beta_z^{TM_z,TE_z}$ and $Z_c^{TM_z,TE_z}$ are the TM_z and TE_z phase constants along the z axis and the characteristic impedances of the line, respectively, and

$$\beta_z^{TM_z} = \pm\sqrt{\omega^2\mu_\rho\varepsilon_z - k_\rho^{TM_z^2}}\sqrt{\frac{\varepsilon_\rho}{\varepsilon_z}}, \tag{5a}$$

$$Z_c^{TM_z} = \frac{\pm\sqrt{\omega^2\mu_\rho\varepsilon_z - k_\rho^{TM_z^2}}}{\omega\varepsilon_\rho}\sqrt{\frac{\varepsilon_\rho}{\varepsilon_z}}, \tag{5b}$$

and

$$\beta_z^{TE_z} = \pm\sqrt{\omega^2\mu_z\varepsilon_\rho - k_\rho^{TE_z^2}}\sqrt{\frac{\mu_\rho}{\mu_z}}, \tag{6a}$$

$$Z_c^{TE_z} = \frac{\omega\mu_z}{\pm\sqrt{\omega^2\mu_z\varepsilon_\rho - k_\rho^{TE_z^2}}}\sqrt{\frac{\mu_\rho}{\mu_z}}, \tag{6b}$$

where $k_\rho^{TM_z,TE_z} = \mathrm{Re}(k_\rho^{TM_z,TE_z}) + j\mathrm{Im}(k_\rho^{TM_z,TE_z})$ are the TM_z and TE_z transverse wave numbers. For later convenience, we also introduce the lighter notations $\mathrm{Re}(k_\rho^{TM_z,TE_z}) = \beta_\rho$ and $\mathrm{Im}(k_\rho^{TM_z,TE_z}) = \alpha_\rho$.

[11] Equations (5) and (6) are extended transmission line parameters for an anisotropic substrate. They reduce to the standard expressions in the particular case of a conventional isotropic slab [see *Felsen and Marcuvitz*, 1996].

[12] In equation (4) $Z_{c0}^{TM_z,TE_z}$ are the TM_z or TE_z free-space characteristic impedances, respectively,

$$Z_{c0}^{TM_z} = \frac{k_{z0}^{TM_z}}{\omega\varepsilon_0}, \tag{7a}$$

$$Z_{c0}^{TE_z} = \frac{\omega\mu_0}{k_{z0}^{TE_z}}, \tag{7b}$$

where $k_{z0}^{TM_z,TE_z} = \mathrm{Re}(k_{z0}^{TM_z,TE_z}) + j\mathrm{Im}(k_{z0}^{TM_z,TE_z})$ are the TM_z and TE_z free-space wave numbers along z and

$$k_{z0}^{TM_z,TE_z} = \pm\sqrt{\omega^2\mu_0\varepsilon_0 - k_\rho^{TM_z,TE_z^2}}. \tag{8}$$

[13] The dispersion relations of equation (4) are transcendental. The explicit k_ρ and k_{z0} dispersion curves are obtained numerically by computing their roots versus frequency.

4. Dispersion Analysis

[14] In this section, we investigate the effects of uniaxial anisotropy (equations (1a) and (1b)) and medium dispersion (equations (2) and (3)) on the behavior (equation (4)) of the uniaxially anisotropic grounded slab. In order to discriminate these two effects, we first consider the effect of uniaxial anisotropy only (even if such a medium does not exist physically) in section 4.1. Later, we add the medium dispersion to determine its specific effect in section 4.2.

4.1. Effect of Uniaxial Anisotropy (Nondispersive Medium)

[15] Three case studies will be performed here, two for TM_z modes and one for TE_z modes. For the TM_z modes, we first keep μ_ρ/μ_z constant and vary $\varepsilon_\rho/\varepsilon_z$, to investigate the effect of electric anisotropy. Next (second case), we keep $\varepsilon_\rho/\varepsilon_z$ constant and vary μ_ρ/μ_z, to investigate the effect of magnetic anisotropy. We also consider two different values of $\varepsilon_\rho/\varepsilon_z$ to determine the combined effects of magnetic and electric anisotropies. In the third study, for the TE_z modes, we vary only μ_ρ/μ_z in equations (4) and (6), since this is the only

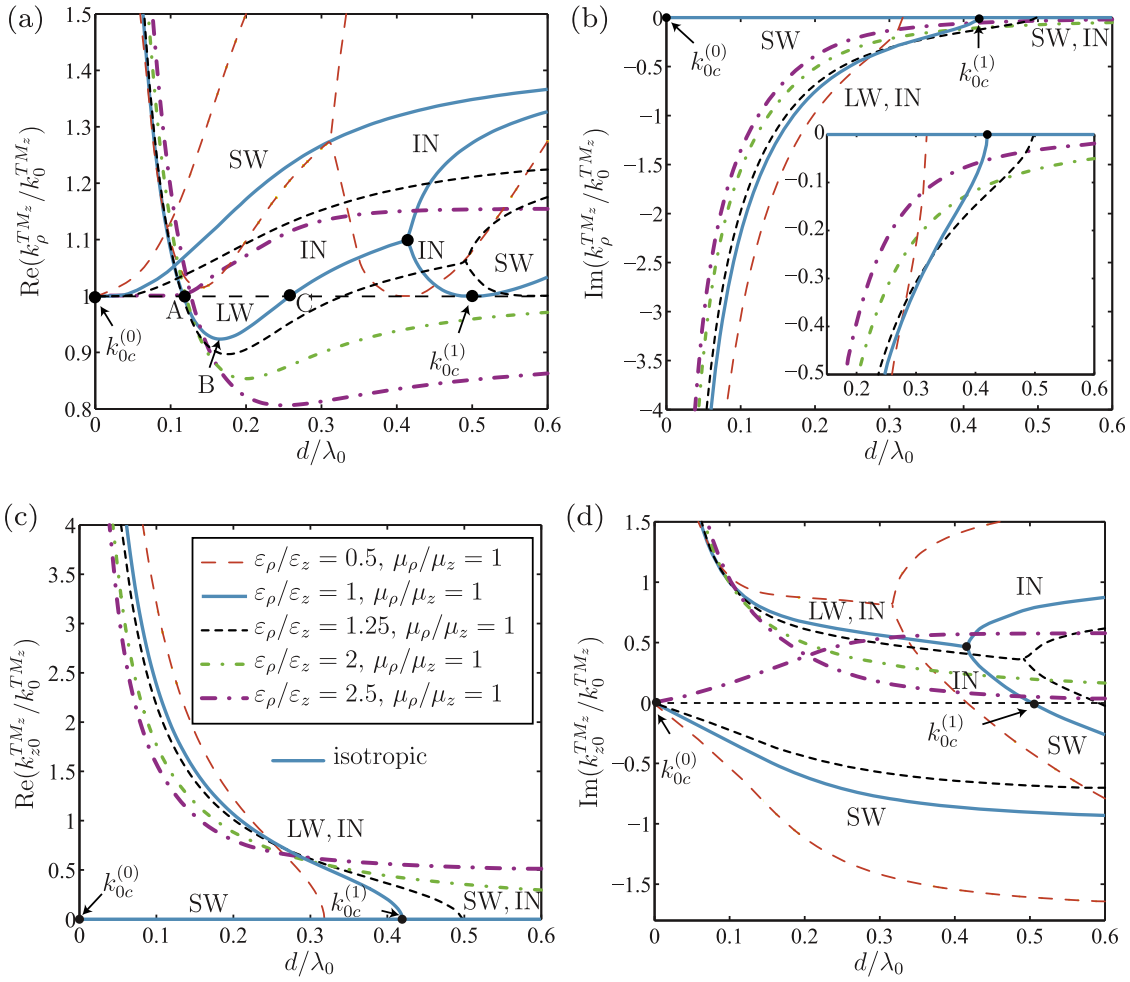

Figure 3. TM_z dispersion curves for the uniaxial anisotropic grounded slab with $\varepsilon_\rho = 2\varepsilon_0$ and $\mu_z = \mu_0$, for a fixed μ_ρ/μ_z and various $\varepsilon_\rho/\varepsilon_z$. (a) $\mathrm{Re}(k_\rho^{TM_z}/k_0^{TM_z})$. (b) $\mathrm{Im}(k_\rho^{TM_z}/k_0^{TM_z})$. (c) $\mathrm{Re}(k_{z0}^{TM_z}/k_0^{TM_z})$. (d) $\mathrm{Im}(k_{z0}^{TM_z}/k_0^{TM_z})$. The surface wave (SW), leaky wave (LW), and improper nonphysical (IN) modes are indicated on the curves for the isotropic case. These indications also apply to Figures 4 and 5.

parameter related to anisotropy. The three case studies also consider the case of an isotropic grounded slab for comparison.

[16] The first case study (TM_z modes, fixed $\mu_\rho/\mu_z = 1$ and varying $\varepsilon_\rho/\varepsilon_z$) is presented in Figure 3. Figure 3 explicitly indicates, on the dispersion curves of the isotropic case, the surface waves modes (SW), the leaky wave modes (LW), and the improper nonphysical modes (IN) [see *Oliner and Jackson*, 2007]. These indications are not repeated but can be easily inferred in the cases of Figures 4 and 5.

[17] Figure 3 (especially Figure 3a) shows that as $\varepsilon_\rho/\varepsilon_z$ increases, the bandwidth of the surface waves modes decreases progressively until they fully transform into leaky modes.

[18] Moreover, the slopes of the resulting leaky modes progressively decrease as $\varepsilon_\rho/\varepsilon_z$ increases, and become almost perfectly flat for electrically very thick slabs, roughly for $d/\lambda_0 > 1/2$ for the parameters considered (λ_0 is the free-space wavelength). This flattening of the dispersive curves has important physical implications and interests for leaky wave antennas. First, since the radiation angle of the main beam of a leaky wave structure is given by $\theta(\omega) \approx \sin^{-1}[\beta_\rho/k_0]$ [see *Oliner and Jackson*, 2007], a flat dispersion curve (i.e., a constant β_ρ/k_0 ratio) leads to a *fixed radiation beam* over a broad bandwidth. This resolves the issue of beam squinting while preserving the leaky wave benefit of high directivity. This is beneficial to broadband point-to-point communication and sensing applications, where a broadband signal should radiate to a fixed direction without experiencing spatial dispersion of its energy across its spectrum.

[19] Figure 4 shows the results of the second case study (TM_z, fixed $\varepsilon_\rho/\varepsilon_z$ and varying μ_ρ/μ_z). It is seen that the leaky dispersion curves progressively flatten as μ_ρ/μ_z is decreased. Moreover, as expected form the previous study, larger $\varepsilon_\rho/\varepsilon_z$ leads to flatter curves. Therefore, it may be concluded that the flattest (i.e., lowest dispersive) TM response is obtained by maximizing $\varepsilon_\rho/\varepsilon_z$ and minimizing μ_ρ/μ_z.

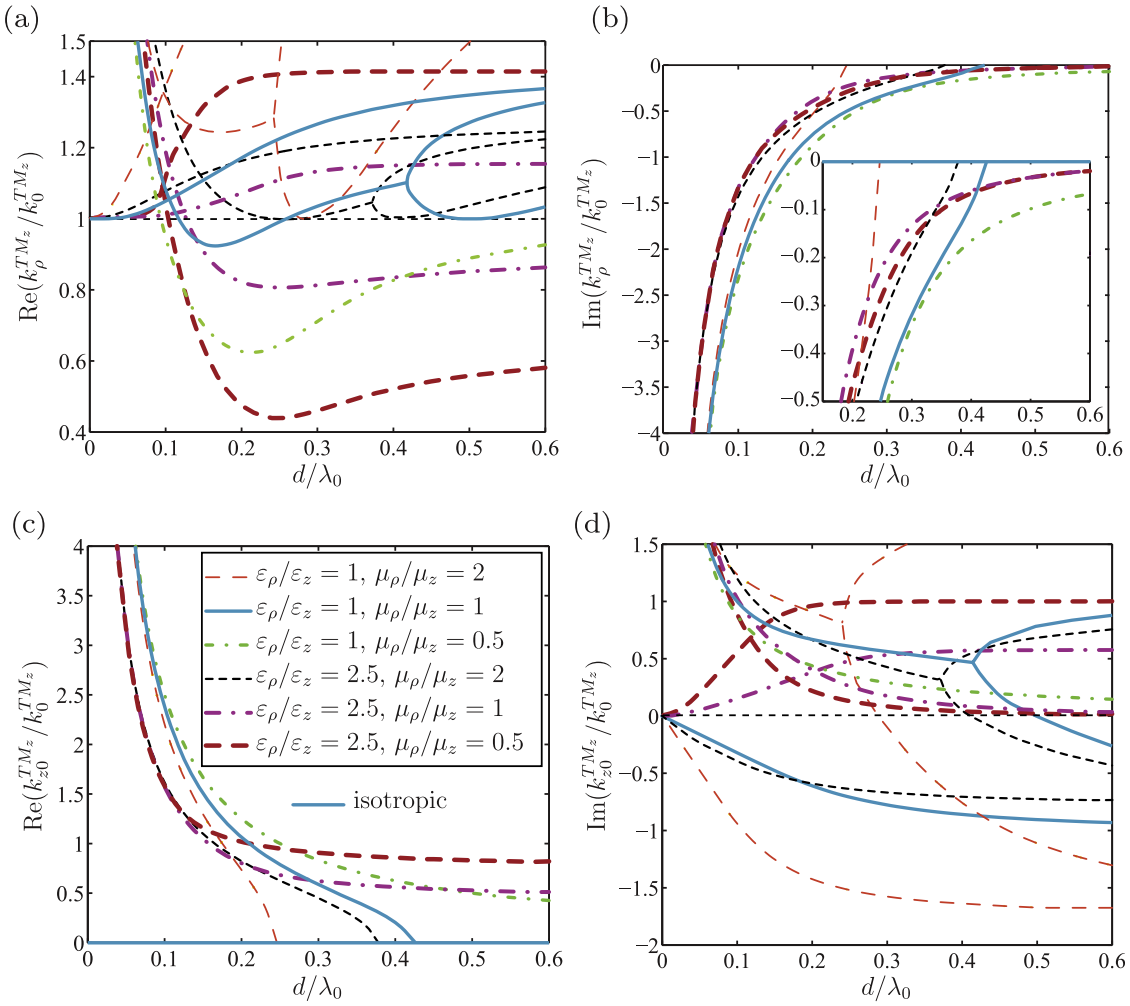

Figure 4. TM_z dispersion curves for the uniaxial anisotropic grounded slab with $\varepsilon_\rho = 2\varepsilon_0$ and $\mu_z = \mu_0$, for a fixed $\varepsilon_\rho/\varepsilon_z$ and various μ_ρ/μ_z. (a) $\mathrm{Re}(k_\rho^{TM_z}/k_0^{TM_z})$. (b) $\mathrm{Im}(k_\rho^{TM_z}/k_0^{TM_z})$. (c) $\mathrm{Re}(k_{z0}^{TM_z}/k_0^{TM_z})$. (d) $\mathrm{Im}(k_{z0}^{TM_z}/k_0^{TM_z})$.

[20] Figure 5 presents the third case study (TE_z, varying μ_ρ/μ_z).

[21] We observe that the TE_z leaky modes have a very different behavior than the TM_z leaky modes. Here, as μ_ρ/μ_z decreases, the dispersion curves penetrate deeper into the leaky wave region but they also become more dispersive. Less dispersion flatting is achievable as compared to the TM_z case for a given slab electrical thickness, which makes these modes less attractive for low-beam squint leaky wave antenna applications. Therefore, in the following, only the TM_z case will be considered.

4.2. Effect of Drude/Lorentz Dispersion in Addition to Anisotropy

[22] Section 4.1 showed that introducing a uniaxial anisotropy of the type given by equations (1a) and (1b) into a grounded slab could generate a very broadband quasi nondispersive leaky wave TM_z mode, of interest for the low-beam squint radiation of broadband signals. However, as pointed out in section 2, the uniaxially anisotropic medium of practical interest are frequency dispersive. So, the question as whether these properties of the grounded slab are preserved in the real case, where the medium exhibits frequency dispersion (in addition to anisotropy), naturally arises. This question will be addressed now.

[23] The permittivity and permeability dispersion curves, given by equations (2) and (3), respectively, for the medium of interest (section 2), are plotted in Figure 6 for the parameters indicated in the caption (lossless case). The permittivity plasma frequency ω_{pe} and the permeability resonant plasma frequency ω_{pm} are designed to be equal, $\omega_{pe} = \omega_{pm} = \omega_p$, so as to avoid the presence of a stop band between the double-negative and double-positive ε_z and μ_ρ frequency ranges. Moreover, the value ω_p ($f = 11$ GHz) was chosen to coincide with the leaky wave cutoff frequency of the isotropic nondispersive grounded slab.

[24] The TM_z dispersion curves of the dispersive uniaxially anisotropic grounded slab with the medium dispersion of Figure 6 are shown in Figure 7. They are compared with the isotropic nondispersive (in terms of the slab medium) and the anisotropic nondispersive (in terms of the slab medium) cases.

[25] Figure 7 reveals that the low-beam squint property is preserved after the introduction of real medium dispersion,

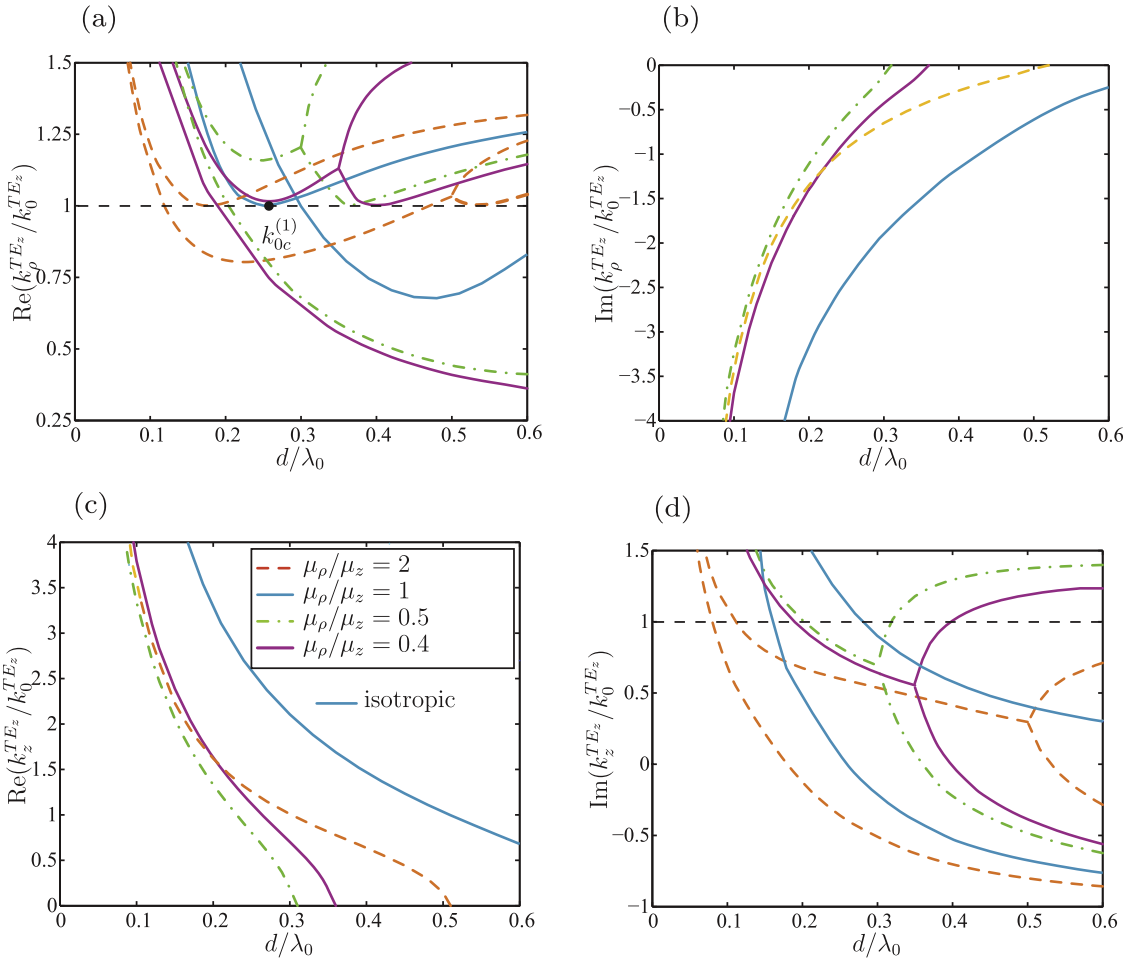

Figure 5. TE_z dispersion curves for the uniaxial anisotropic grounded slab with $\varepsilon_\rho = 2\varepsilon_0$ and $\mu_z = \mu_0$, for a fixed $\varepsilon_\rho/\varepsilon_z = 1$ and various μ_ρ/μ_z. (a) $\mathrm{Re}(k_\rho^{TE_z}/k_0^{TE_z})$. (b) $\mathrm{Im}(k_\rho^{TE_z}/k_0^{TE_z})$. (c) $\mathrm{Re}(k_z^{TE_z}/k_0^{TE_z})$. (d) $\mathrm{Im}(k_z^{TE_z}/k_0^{TE_z})$.

since the anisotropic dispersive (physical) curves still remain very flat.

[26] The magnitude of the leakage factor of the anisotropic dispersive mode is comparable to that of a typical leaky wave antenna, thus allowing high-directivity leaky wave radiation [see *Oliner and Jackson*, 2007].

5. Far-Field Radiation Analysis

5.1. Green's Functions for Vertical Point Source

[27] Section 4 revealed that the TM_z modes are appropriate for broadband, highly directive and low-beam squint leaky wave radiation. Such TM_z modes may be excited by a vertical point source excitation embedded in the substrate, as shown in Figure 8a. This excitation reads in the spectral domain $\tilde{\mathbf{J}} = 1/(2\pi)\delta(z - z')\mathbf{a}_z$. The corresponding equivalent transmission line model is shown in Figure 8b, where the vertical point source is modeled by the series voltage source $V_g = |\tilde{\mathbf{J}}| = J_z$ [see *Grzegorczyk and Mosig*, 2003]. Using Sommerfeld's choice for the potentials [see *Mosig*, 1989], the far fields can be entirely determined by the $\tilde{G}_A^{zz}$ component of the spectral-domain magnetic vector potential dyadic Green's function $\bar{\bar{G}}_A$.

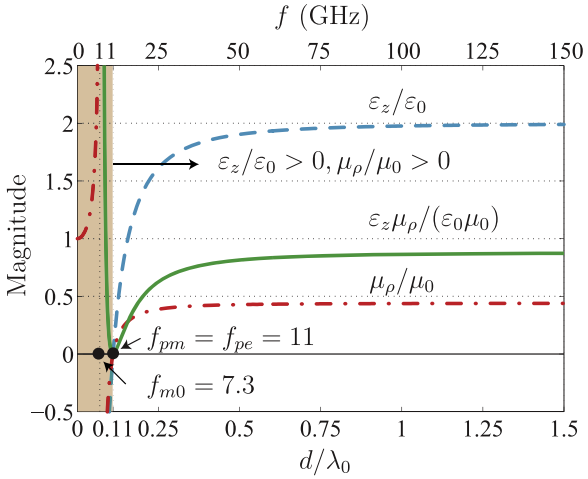

Figure 6. Dispersive response for the permittivity $\varepsilon_z/\varepsilon_0$ (Drude model) (equation (2)) and permeability μ_ρ/μ_0 (Lorentz model) (equation (3)) for equal electric and magnetic plasma frequencies ($\omega_{pe} = \omega_{pm}$). The parameters are $F = 0.56$, $\omega_{m0} = 2\pi \times 7.3 \times 10^9$ rad/s, fixing $\omega_{pm} = \omega_{m0}/\sqrt{1-F} = 2\pi \times 11 \times 10^9$ rad/s, $\varepsilon_r = 2$, $\omega_{pe} = \omega_{pm}$, $\zeta_e = 0$ and $\zeta_m = 0$. The substrate thickness is $d = 3$ mm.

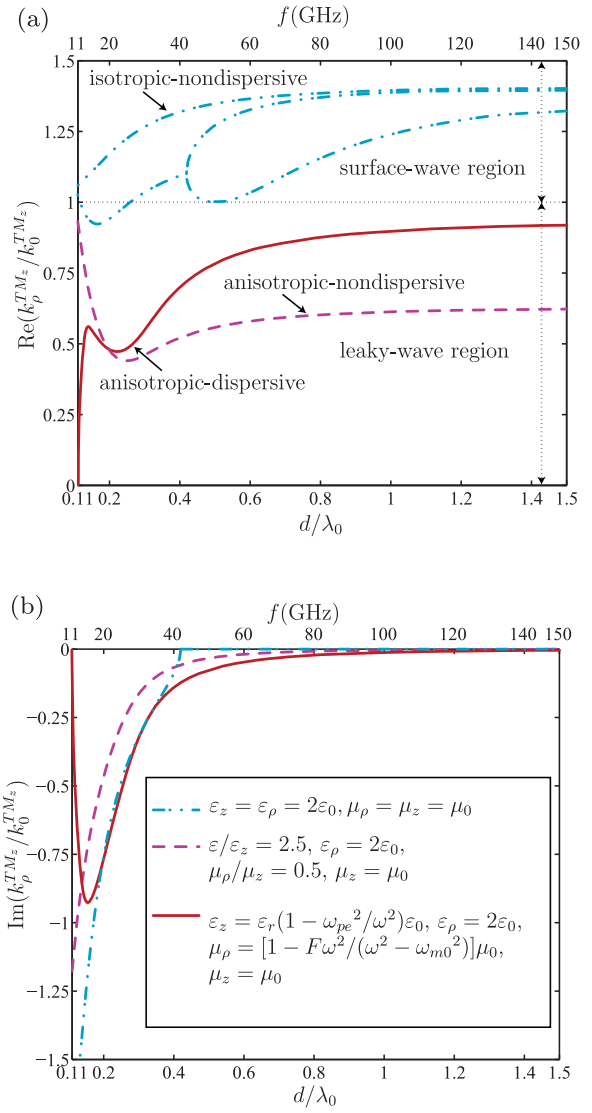

Figure 7. Comparison of the dispersions of the first TM_z leaky modes for different grounded slabs: nondispersive (slab medium) isotropic ($\varepsilon_z = \varepsilon_\rho = 2\varepsilon_0$, $\mu_\rho = \mu_z = \mu_0$), nondispersive (slab medium) anisotropic ($\varepsilon_\rho/\varepsilon_z = 2.5$, $\varepsilon_\rho = 2\varepsilon_0$, $\mu_\rho/\mu_z = 0.5$, $\mu_z = \mu_0$), and dispersive anisotropic ($\varepsilon_z = \varepsilon_r(1 - \omega_{pe}^2/\omega^2)\varepsilon_0$, $\varepsilon_\rho = 2\varepsilon_0$, $\mu_\rho = [1 - F\omega^2/(\omega^2 - \omega_{m0}^2)]\mu_0$, $\mu_z = \mu_0$). (a) Re($k_\rho^{TM_z}/k_0^{TM_z}$). (b) Im($k_\rho^{TM_z}/k_0^{TM_z}$). The nonspecified parameters are equal to those of Figure 6.

[28] By substituting equations (1) into the spectral-domain Maxwell's equations with the above source $\tilde{\mathbf{J}}$ and manipulating the resulting relations, the following relevant equations are found

$$\frac{d^2}{dz^2}\left[\frac{-\omega\varepsilon_z}{k_x^{TM_z}}\tilde{G}_{EJ}^{xz,TM_z}\right] = -\frac{\varepsilon_\rho}{\varepsilon_z}k_z^{TM_z^2}\left[\frac{-\omega\varepsilon_z}{k_x^{TM_z}}\tilde{G}_{EJ}^{xz,TM_z}\right] + \frac{d}{dz}\tilde{J}_z, \tag{9a}$$

$$\frac{d}{dz}\left[\frac{-\omega\varepsilon_z}{k_x^{TM_z}}\tilde{G}_{EJ}^{xz,TM_z}\right] = -j\frac{k_z^{TM_z}}{\omega\varepsilon_z}k_z^{TM_z}\left[\frac{-\omega^2\varepsilon_z^2}{k_\rho^{TM_z^2}}\tilde{G}_{EJ}^{zz,TM_z}\right], \tag{9b}$$

to map the transmission line equations

$$\frac{d^2\tilde{V}}{dz^2} + ZYk_z^2\tilde{V} = \frac{dV_g}{dz}, \tag{10a}$$

$$\frac{d\tilde{V}}{dz} = -jZk_z\tilde{I}. \tag{10b}$$

By identifying equation (10a) with equation (9a) and equation (10b) with equation (9b), we next obtain the Green's functions

$$\tilde{G}_{EJ}^{xz,TM_z} = \frac{-k_x^{TM_z}}{\omega\varepsilon_z}\tilde{V}, \tag{11a}$$

$$\tilde{G}_{EJ}^{zz,TM_z} = \frac{-k_\rho^{TM_z^2}}{\omega^2\varepsilon_z^2}\tilde{I}, \tag{11b}$$

where $\tilde{V}$ and $\tilde{I}$ are the spectral domain voltage and current along the equivalent transmission line (see Figure 8b). Next, the relevant magnetic field Green's function components are obtained by substituting equations (11) into Maxwell's equations

$$\tilde{G}_{HJ}^{xz,TM_z} = \frac{k_y^{TM_z}}{\omega\varepsilon_z}\tilde{I}, \tag{12}$$

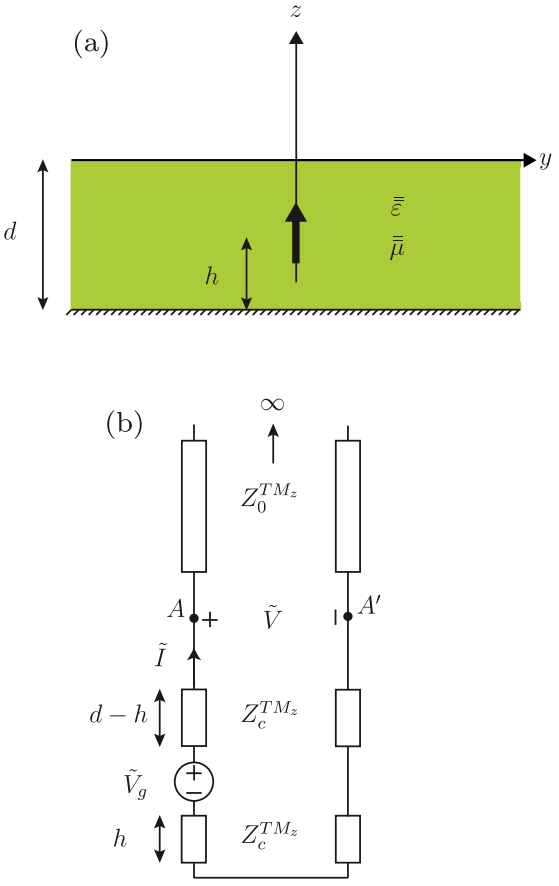

Figure 8. Uniaxially anisotropic grounded slab excited by an embedded vertical point source. (a) Physical structure. (b) Transmission line model.

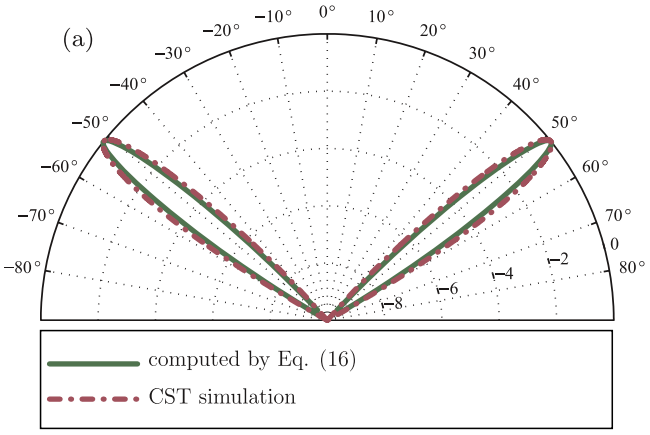

Figure 9. Radiation pattern for a vertical point source located at h = 1.5 mm from the ground plane in the anisotropic grounded slab (Figure 8a) at f = 51 GHz where $k_\rho/k_0 = 0.78 - j0.07$ (Figure 7) for the parameters of Figure 6. (a) Comparison between theory (equation (16)) and full-wave (FIT-CST) simulation results. (b) Three-dimensional conical pattern.

while $\tilde{G}_{HJ}^{zz,TM_z} = 0$ because it is a TM_z mode. The sought for Green's function $\tilde{G}_A^{zz}$ is finally obtained by inverting the relation

$$\overline{\overline{\mathbf{G}}}_{HJ} = \overline{\overline{\mu}}^{-1} \nabla \times \overline{\overline{\mathbf{G}}}_A, \tag{13}$$

which yields

$$\tilde{G}_A^{zz} = \frac{-j\mu_\rho}{\omega \varepsilon_z} \tilde{I}. \tag{14}$$

[29] These Green's functions have been computed following the same procedure as in the work by *Grzegorczyk and Mosig* [2003] with extension to the case of uniaxial anisotropy.

5.2. Asymptotic Far-Field Expressions

[30] The far field radiated by a z-directed source in a layered medium may be written in terms of the corresponding Green's function at the interface with air (at AA' in Figure 8b), $\tilde{G}_A^{zz}(k_x, k_y)$, as $\tilde{g}_A^{zz}(k_x, k_y, z) = \tilde{G}_A^{zz}(k_x, k_y) \exp(-jk_{z0}z)$. The double Fourier transform relating the spectral to the spatial domain Green's function reduces then to the value of the integrand at the saddle point [see *Felsen and Marcuvitz*, 1996; *Mosig and Gardiol*, 1982; *Collin*, 1991], resulting in

$$g_A^{zz}(k_x, k_y, z) = jk_0 \cos\theta \tilde{G}_A^{zz}(k_x, k_y) \frac{\exp(-jk_0 r)}{r}. \tag{15}$$

The electric field is then calculated from equation (15) as follows [see *Mosig*, 1989]

$$E_\theta(x, y, z) = \frac{-1}{2} \omega k_0 \sin(2\theta) \tilde{G}_A^{zz}(k_x, k_y) \frac{\exp(-jk_0 r)}{r}, \tag{16}$$

while $E_\phi(x, y, z) = 0$. Equation (16) represents the complete far field, which includes contributions from leaky waves, related to the poles of $\tilde{G}_A^{zz}(k_x, k_y)$ [see *Collin*, 1991], and from the space wave, corresponding to the direct radiation of the dipole to free space through the substrate.

[31] Figure 9a compares the theoretical (equation (16)) and full wavefields, obtained with CST, radiated by a vertical point source. This source is located at h = 1.5 mm from the ground plane in the anisotropic grounded slab (Figure 8a) at f = 51 GHz, where $k_\rho/k_0 = 0.78 - j0.07$ (Figure 7) for the parameters of Figure 6. The CST setup emulates the theoretical infinite substrate by a grounded slab of $35\lambda_0 \times 35\lambda_0$ mm terminated by open boundaries, and emulates the point source by a small discrete current source. Figure 9a shows good agreement between theoretical and full-wave results, thus validating the theory presented.

6. Leaky Wave Properties Discussion

[32] In this section, the behavior and the performance of isotropic and double anisotropic (i.e., anisotropic in terms of both the permittivity and permeability) grounded slabs excited by a vertical point source are compared with the help of the dispersion and the far-field radiation results presented in sections 4 and 5.2, respectively.

6.1. Inappropriateness of the Isotropic Structure

[33] The leaky wave radiation from an isotropic grounded slab has several important limitations, due to the following reasons.

[34] 1. The leaky wave pointing angle θ_p is restricted to a small angular range near end-fire. For instance, this range is limited to 68° − 90° in Figure 10a. This represents a severe limitation in planar antenna applications, where radiation capability close to broadside is usually required, particularly in flush-mounted antenna systems including obstacles in the plane of the antenna. This angular range restriction of θ_p is related, via the scanning law $\theta_p \simeq \sin^{-1}(\beta_\rho/k_0)$ [see *Oliner and Jackson*, 2007], to the fact that the phase constant β_ρ, cannot reach values significantly smaller than k_0, as shown in Figure 10a. This is due to the relatively small permittivity (ε_r = 2 in Figure 10a) of the slab. At small permittivities, leakage to free space is eased by the fact that the wave experiences little trapping inside the slab (no trapping at all in the limiting case $\varepsilon_r \to 1$). As a result, the leakage factor α_ρ (radiation per unit length) is also relatively large, since all the energy tends to radiate directly from the dipole. This behavior is apparent in Figure 3a (solid blue curve). Leakage

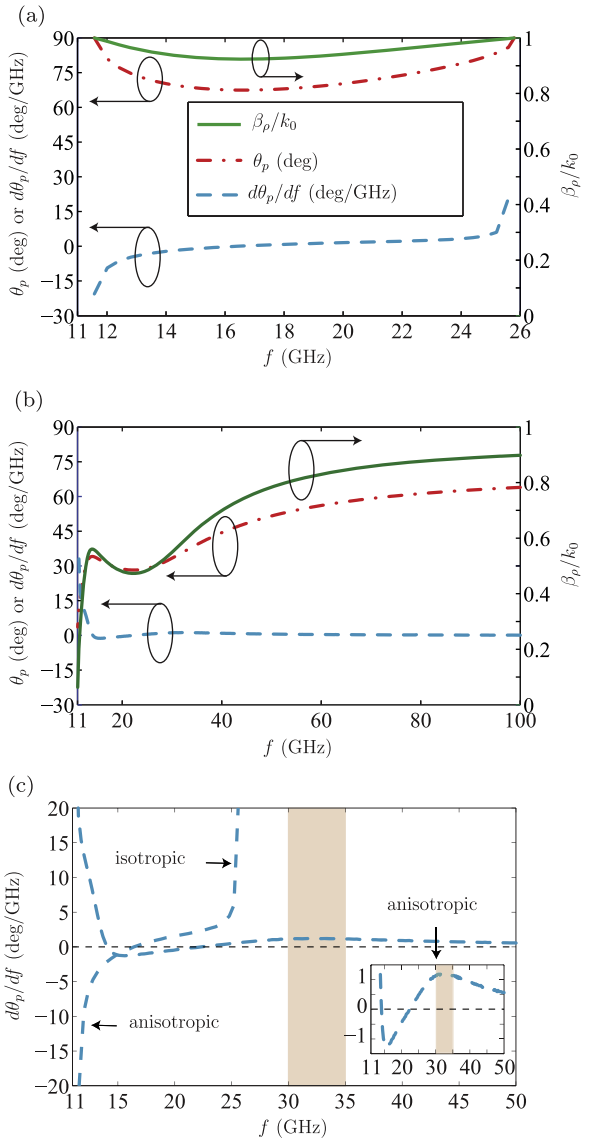

Figure 10. Pointing angle of the leaky mode and its variation over frequency calculated from $\theta_p = \sin^{-1}(\beta_\rho/k_0)$ [see *Oliner and Jackson*, 2007] for the slab with the dispersion curves of Figure 7 and $d = 3$ mm. (a) Isotropic slab with $\varepsilon_z = \varepsilon_\rho = 2\varepsilon_0$, $\mu_\rho = \mu_z = \mu_0$. (b) Anisotropic slab with $\varepsilon_z = \varepsilon_r(1 - \omega_{pe}^2/\omega^2)\varepsilon_0$, $\varepsilon_\rho = 2\varepsilon_0$, $\mu_\rho = [1 - F\omega^2/(\omega^2 - \omega_{m0}^2)]\mu_0$, $\mu_z = \mu_0$. (c) Comparison of the variations of the pointing angle with respect to frequency for the isotropic and anisotropic substrates.

occurs along the valley-like dispersion curve between points A and C in this graph. As the electrical thickness of the substrate decreases below C, β_ρ decreases to reach a minimum in the leaky wave region at B. Then, the curve increases again toward k_0 to finally penetrate into the nonphysical region at A. As the permittivity increases, the wave becomes more and more trapped inside the slab, and tends to propagate at smaller angles (smaller β_ρ). This results in a deeper penetration into the leaky wave region, leading to smaller angles of radiation toward the broadside direction, as shown in Figure 11. However, the extension in the scanning range is accompanied with a severe loss of directivity and bandwidth reduction, as will be shown below.

[35] 2. Due to the effect of wave guidance in the slab, the far-field radiation exhibits a null at end-fire, as shown by the cos θ factor in equation (15). Therefore, due to this angular factor *the contribution of the leaky wave to the total radiation tends to be suppressed*, since directive and useful leaky wave radiation occurs only near end-fire according to the previous point. As a consequence, radiation is mostly dominated by a space wave, whose beam direction is dictated by the electrical thickness of the substrate. Figure 12 shows the radiation patterns for the isotropic slab computed by equation (16) for various frequencies along the leaky wave dispersion curve of Figure 10a and at one nonphysical frequency where no leaky wave can exist (Figure 7a). Figure 12 shows that the radiation angles at these frequencies point at around $\theta = 45°$, which does not correspond at all to the angles predicted by the leaky wave scanning law in Figure 10a. This also applies to the nonphysical grounded slab frequency (27 GHz). Thus, radiation is not due to the leaky wave but to the space wave. Such a wave does not allow scanning and provides little radiation directivity, as discussed in the next point.

[36] 3. The directivity of the structure is low ($D = 6.61$ dBi at $f = 24.2$ GHz in Figure 12). The leaky-mode radiation, in addition to being limited to the end-fire region, also exhibits a very poor directivity due to the large magnitude of its leakage factor $|\alpha_\rho|$, as shown in Figure 7b. As a result, the aperture size becomes extremely small, which leads to a very

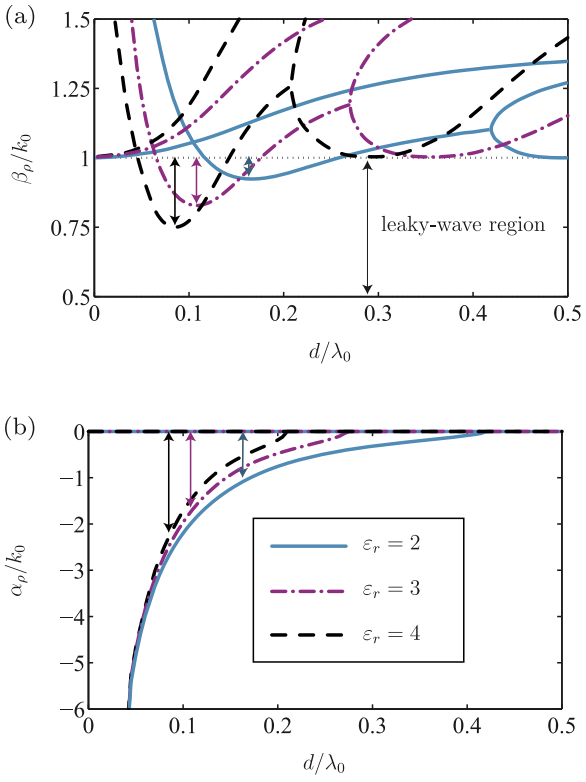

Figure 11. Comparison of the leaky wave behavior of the isotropic grounded slab for different permittivities ($\varepsilon_r = 2, 3, 4$), with $\mu_r = 1$ and $d = 3$ mm.

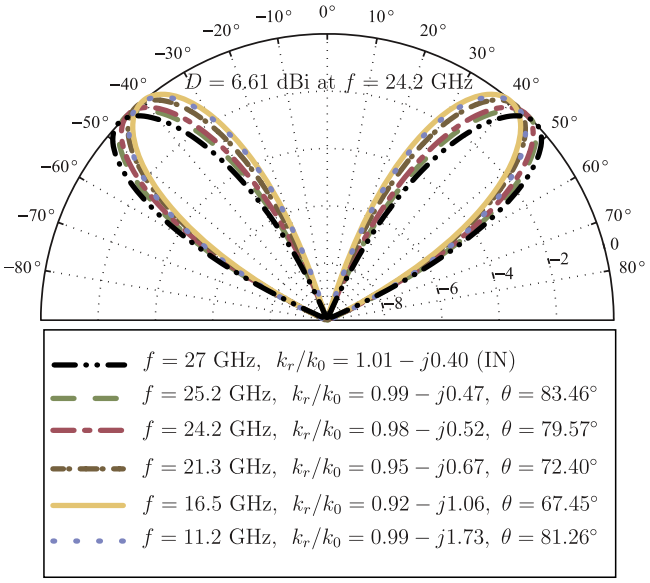

Figure 12. The radiation from an isotropic grounded slab for various frequencies from Figure 10a and for the frequency of f = 27 GHz, which lies in the improper nonphysical (IN) region of the dispersion curve of Figure 7.

low directivity. On the other hand, the space wave, producing the pattern shown in Figure 12, also does not provide high directivity due to its direct radiation to free space.

[37] 4. The radiation efficiency (both for the leaky and space waves) is further reduced by the propagation of the first (cutoffless) TM_0 surface mode at all frequencies (especially higher), as shown in Figure 7a. This surface mode not only reduces the efficiency by forcing the guidance of part of energy from the source, but also generates diffraction at the end of a practical substrate, which induces back radiation and spurious ripples in the forward radiation pattern.

[38] 5. The leaky-mode bandwidth is very narrow. In fact, there is a trade-off between bandwidth and minimum pointing angle, as shown in Figure 11. Larger bandwidths are achievable with lower permittivities, but this restricts the pointing angle to the deep end-fire region. Figure 13 further reveals that the leaky-mode bandwidth decreases as the permittivity is increased, as a result of the decrease of the critical angle of total internal reflection in the substrate (red line in Figure 13).

[39] Following the above discussion on the pointing angle, Figure 14 confirms that increasing the slab permittivity decreases the minimum pointing angle (and thereby also increases the scanning range toward broadside since near-end-fire radiation is always present around the leaky wave to surface wave transition region). Figure 14 further confirms the subsequent increase of the leakage factor, which results in a decrease of the directivity.

[40] The points discussed above are general, and the leaky wave performances of the isotropic grounded slab structure cannot be significantly improved beyond the presented results.

6.2. Appropriateness and Performance of the Double Anisotropic Structure

[41] We now explore the leaky wave radiation properties of the dispersive double anisotropic grounded slab, showing the advantages over the isotropic substrate.

[42] 1. A wide range of beam pointing angles is available, from broadside almost to end-fire. For example, in Figure 10b, this range extends from 0° to 65°. The reason for this wide scanning range is apparent in Figure 6, where $0 \le \varepsilon_z\mu_\rho/(\varepsilon_0\mu_0) < 1$, and therefore $0 \le \beta_\rho/k_0 < 1$, in the leaky-mode range. In this case, the largest pointing angle is limited to 65° because of the asymptotic behavior of $\varepsilon_z\mu_\rho/(\varepsilon_0\mu_0) \overset{\omega\to\infty}{=} 0.88$, corresponding to $\beta_\rho/k_0 \overset{\omega\to\infty}{=} 0.9$. Larger pointing angles can be achieved by increasing the effective index $\varepsilon_z\mu_\rho$ to values exceeding unity at some frequency, so that β_ρ reaches k_0 (at the transition region from the leaky mode to the surface mode). This is shown in Figure 15, where the maximum pointing angle $\theta_{p,\max}$, and therefore also the scanning range of the leaky mode is increased by increasing the permittivity of the host medium, ε_r, so as to scan the entire angular range from 0° to 90° (this occurs for a permittivity close to $\varepsilon_r = 2.5$). Figure 16 shows the scanning behavior of the leaky mode over the broad frequency range of 11 GHz to 150 GHz. Note the null at broadside, which is due to the vertical point source excitation.

[43] 2. The directivity of the leaky wave radiation may be very high. Figure 7b shows that the magnitude of the leakage factor, $|\alpha_\rho|$, becomes very small as frequency increases, thereby allowing a large radiating aperture and a very directive beam. Figure 16 shows that, according to the behavior of the leakage factor in Figure 7b, the beam becomes extremely directive as the frequency increases.

[44] 3. The radiation efficiency of the anisotropic substrate is much higher than that for the isotropic structure, since no surface modes exist in the leaky-mode frequency range, as shown in Figure 7a. Therefore no energy is coupled inside the dielectric through the surface modes. In the case of the isotropic substrate, the TM_0 surface mode is always present in addition to the leaky mode (see also Figure 7a).

[45] 4. The bandwidth of the leaky mode is wider than that for the isotropic structure, as seen in Figure 7a. Figure 6 shows that $\lim_{\omega\to\infty} \varepsilon_z\mu_\rho/(\varepsilon_0\mu_0) < 1$ in the right-handed frequency range. For the reason explained above, this fact

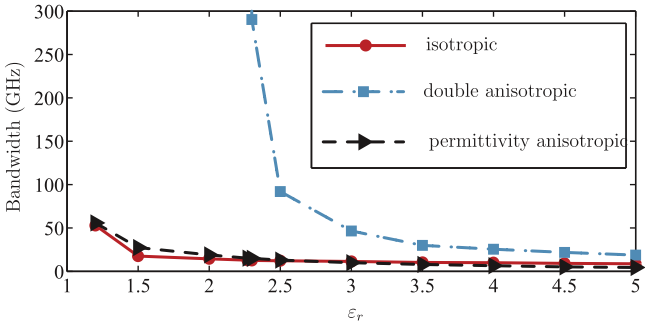

Figure 13. Comparison of the leaky wave bandwidth versus the host medium permittivity ε_r between the isotropic, double anisotropic, and permittivity-only anisotropic grounded slabs.

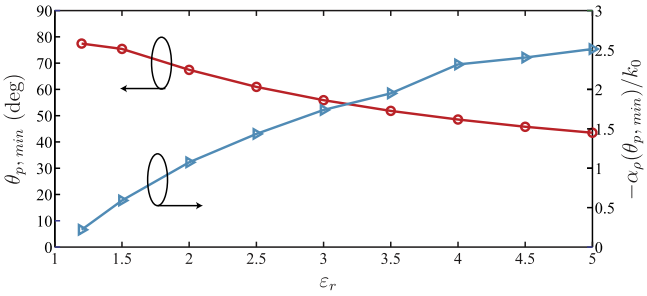

Figure 14. Minimum pointing angle $\theta_{p,\min}$ for the isotropic substrate versus the permittivity ε_r and corresponding leakage factor α $(\theta_{p\min})/k_0$.

prevents radiation at end-fire (practically not very useful anyways), but leads to a huge frequency band of operation. Figure 13 shows that by increasing the host medium permittivity ε_r, the bandwidth of the leaky mode decreases as a consequence of the increasing importance of surface modes. This effect also occurs in the isotropic case, but the double anisotropic structure always exhibits a much wider bandwidth.

[46] 5. The beam squinting is extremely low. This is a direct consequence of the previous point. Figure 10c compares the beam squinting $d\theta_p/df$ of the leaky mode for the isotropic and double anisotropic structures. Close to the plasma frequency (f = 11 GHz), the beam squinting of the isotropic and the anisotropic structures are comparable. However, for the anisotropic case, it quickly drops as frequency increases above the plasma frequency; it then reaches a value that is always less than that of the isotropic slab, and remains relatively constant up to very high frequencies. Figure 17 shows the beam squinting of the leaky wave beam for the anisotropic slab in the frequency range of f = 30–35 GHz. In accordance with Figure 10c, the beam squinting in the bandwidth of Δf = 5 GHz is only 7°.

6.3. Importance of the Dispersion Associated With Magnetic Anisotropy

[47] As discussed above, the reason for bandwidth enhancement, and the subsequent reduction of beam squinting, is the fact that $\varepsilon_z\mu_\rho/(\varepsilon_0\mu_0) < 1$ in a wide frequency range, as illustrated in Figure 6. This asymptotic behavior is essentially due to the dispersive contribution of

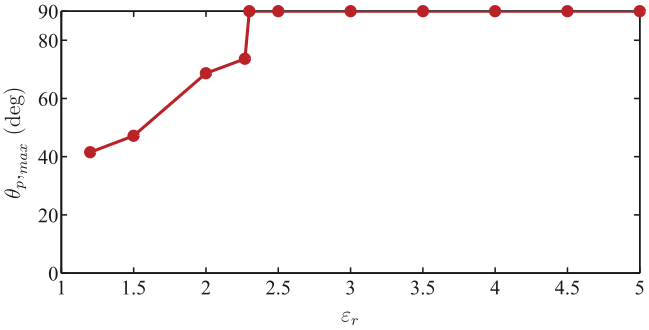

Figure 15. Maximum pointing angle of the leaky-mode radiation from the double anisotropic grounded slab.

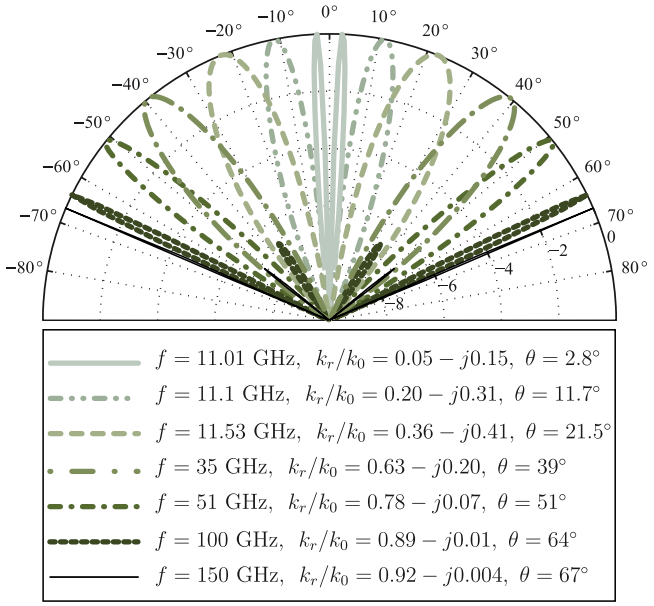

Figure 16. The scanning behavior of the double anisotropic substrate in a wide band frequency range.

μ_ρ since $\lim_{\omega\to\infty} \varepsilon_z/\varepsilon_0 > 1$. Therefore, the dispersive behavior in μ_ρ should satisfy the condition $\lim_{\omega\to\infty} \mu_\rho/\mu_0 < 1$. This magnetic response is inherent to magnetodielectric artificial metasubstrates. Thus, such a performance cannot be achieved with a substrate that would be only electrically artificial but magnetically conventional. This is because for these materials, $\varepsilon_z/\varepsilon_0 < 1$ only occurs in narrow frequency ranges just above the electric plasma frequency. Figure 13 compares the bandwidths of the electrically artificial slab with that of the double electrically and magnetically artificial (anisotropic and dispersive) slabs. It shows that the bandwidth of the only electrically anisotropic slab is similar to the conventional slab, and much smaller than that of the

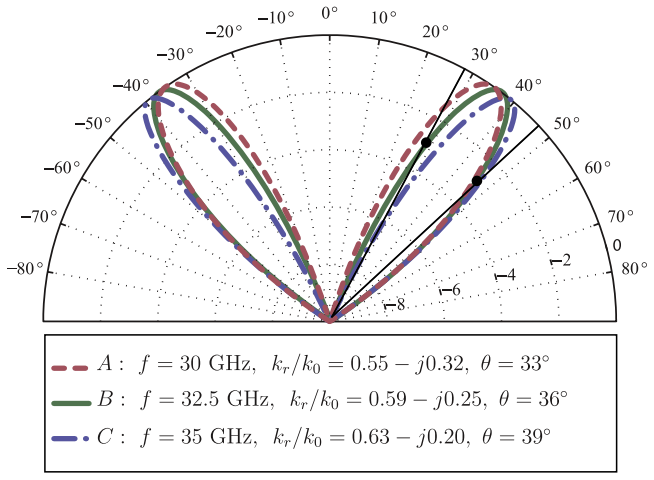

Figure 17. Beam squinting of the leaky-mode radiation of the anisotropic slab of Figure 10b in the bandwidth of Δf = 5 GHz for f = 30–35 GHz.

double anisotropic slab. It is important to note that this behavior cannot either be achieved using a simple ferrite material which has also a Lorentz permeability response [see *Lax and Button*, 1962]. This is because, according to equation (3), in the artificial case the static and infinite frequency limit values of μ_ρ/μ_0 are $\mu_\rho/\mu_0(\omega = 0) = 1$ and $\mu_\rho/\mu_0(\omega \rightarrow \infty) = 1 - F < 1$, respectively (the $\omega \rightarrow \infty$ asymptotic diamagnetic response $\mu_\rho < \mu_0$ is a consequence of Lenz's law). In contrast, in the ferrite case, $\mu_\rho/\mu_0(\omega = 0) > 1$ and $\mu_\rho/\mu_0(\omega \rightarrow \infty) = 1$.

[48] This demonstrates the importance of the Lorentz-type permeability of equation (3) with $\lim_{\omega \rightarrow \infty} \mu_\rho/\mu_0 < 1$, which requires artificial magnetic anisotropy, besides the Drude-type permittivity of equation (2), for very broadband operation.

7. Conclusion

[49] A spectral analysis has been applied to the study of the behavior of leaky and surface modes in anisotropic magnetodielectric metasubstrates.

[50] The analysis has shown, for the first time, that an anisotropic grounded slab provides a highly directive leaky wave radiation with high design flexibility. Toward its lower frequencies, this mode allows full-space conical-beam scanning. At higher frequencies, it provides fixed-beam radiation (at a designable angle) with very low-beam squint, which makes it particularly appropriate for future applications in wide band point-to-point communication and radar systems.

[51] The loss of homogeneity far above the Lorentz resonant frequency in conventional metamaterial substrates, such as the mushroom substrate, would prevent the utilization of the low-beam squint regime of the proposed anisotropic antenna at high frequency. However, it is anticipated that novel periodic structures using unit-cell compression techniques or multiscale nanostructured metamaterials will provide a solution to this issue in the future, henceforth enabling the two operation ranges of the antenna.

References

Allen, C. A., C. Caloz, and T. Itoh (2004), A novel metamaterial-based two-dimensional conical-beam antenna application, in *Proceedings of 2004 IEEE MTT-S International Microwave Symposium Digest*, vol. 1, pp. 305–308, Inst. of Electr. and Electr. Eng., Fort Worth, Tex.

Allen, C. A., K. M. K. H. Leong, C. Caloz, and T. Itoh (2005), A two-dimensional edge excited metamaterial-based leaky wave antenna, in *Proceedings of 2005 IEEE Antennas and Propagation Society International Symposium*, pp. 320–323, Inst. of Electr. and Electr. Eng., Washington, D. C.

Burghignoli, P., G. Lovat, F. Capolino, D. R. Jackson, and D. R. Wilton (2008), Directive leaky-wave radiation from a dipole source in a wire-medium slab, *IEEE Trans. Antennas Propag.*, *56*(5), 1329–1339.

Caloz, C., and T. Itoh (2006), *Electromagnetic Metamaterials: Transmission Line Theory and Microwave Applications*, 1st ed., Wiley-IEEE, Hoboken, N. J.

Caloz, C., T. Itoh, and A. Rennings (2008), CRLH metamaterial traveling-wave and resonant antennas, *IEEE Antennas Propag. Mag.*, *50*(5), 25–39.

Capolino, F. (2009), *Metamaterials Handbook*, CRC Press, Boca Raton, Fla.

Carignan, L. P., A. Yelon, D. Ménard, and C. Caloz (2011), Ferromagnetic nanowire metamaterials: Theory and applications, *IEEE Trans. Microwave Theory Tech.*, in press.

Collin, R. E. (1991), *Field Theory of Guided Waves*, 2nd ed., IEEE Press, New York.

Coulombe, M., H. V. Nguyen, and C. Caloz (2007), Substrate integrated artificial dielectric (SIAD) structure for miniaturized microstrip circuits, *IEEE Antennas Wireless Propag. Lett.*, *6*, 575–579.

Coulombe, M., S. F. Koodiani, and C. Caloz (2010), Compact elongated mushroom (EM)-EBG structure for enhancement of patch antenna array performances, *IEEE Trans. Antennas Propag.*, *58*(4), 1076–1086.

Eleftheriades, G. V. (2007), Enabling RF/microwave devices using negative-refractive-index transmission-line (NRI-TL) metamaterials, *IEEE Antennas Propag. Mag.*, *49*(2), 34–51.

Engheta, N., and R. W. Ziolkowski (2006), *Electromagnetic Metamaterials: Physics and Engineering Explorations*, Wiley-IEEE, New York.

Felsen, L. B., and N. Marcuvitz (1996), *Radiation and Scattering of Waves*, Prentice-Hall, Englewood Cliffs, N. J.

Feresidis, A. P., and J. C. Vardaxoglou (2001), High-gain planar antenna using optimized partially reflective surfaces, *IEE Proc. Microwaves Antennas Propag.*, *148*(6), 345–350.

Grzegorczyk, T. M., and J. R. Mosig (2003), Full-wave analysis of antennas containing horizontal and vertical metallizations embedded in planar multilayered media, *IEEE Trans. Antennas Propag.*, *51*(11), 3047–3054.

Gupta, S., and C. Caloz (2009), Analog signal processing in transmission line metamaterial structures, *Radioengineering*, *18*(2), 155–167.

Hansen, W. W. (1940), Radiating electromagnetic waveguide, Patent 2,402,622, U.S. Patent and Trademark Off., Washington, D. C.

Hines, J. N., and J. R. Upson (1957), *A wide aperture tapered-depth scanning antenna*, Ohio State Univ. Res. Found., Columbus.

Ikonen, P. M. T., K. N. Rozanov, A. V. Osipov, P. Alitalo, and S. A. Tretyakov (2006), Magnetodielectric substrates in antenna miniaturization: Potential and limitations, *IEEE Trans. Antennas Propag.*, *54*(11), 3391–3399.

Ip, A., and D. R. Jackson (1990), Radiation from cylindrical leaky waves, *IEEE Trans. Antennas Propag.*, *38*(4), 482–488.

Jackson, D. R., and A. A. Oliner (1988), A leaky-wave analysis of the high-gain printed antenna configuration, *IEEE Trans. Antennas Propag.*, *36*(7), 905–910.

Jackson, D. R., A. A. Oliner, and A. Ip (1993), Leaky-wave propagation and radiation from a narrow-beam multiple-layer dielectric structure, *IEEE Trans. Antennas Propag.*, *41*(3), 344–348.

Lai, A., C. Caloz, and T. Itoh (2004), Composite right/left-handed transmission line metamaterials, *IEEE Microwave Mag.*, *5*(3), 34–50.

Lax, B., and K. J. Button (1962), *Microwave Ferrites and Ferrimagnetics*, McGraw-Hill, New York.

Lovat, G., P. Burghignoli, F. Capolino, D. R. Jackson, and D. R. Wilton (2006), Analysis of directive radiation from a line source in a metamaterial slab with low permittivity, *IEEE Trans. Antennas Propag.*, *54*(3), 1017–1030.

Marcuvitz, N. (1951), *Waveguide Handbook*, McGraw-Hill, New York.

Mosallaei, H., and K. Sarabandi (2007), Design and modeling of patch antenna printed on magneto-dielectric embedded-circuit metasubstrate, *IEEE Trans. Antennas Propag.*, *55*(1), 45–52.

Mosig, J. R. (1989), *Integral Equation Techniques*, Wiley Intersci., New York.

Mosig, J. R., and F. E. Gardiol (1982), *Advances in Electronics and Electron Physics*, Academic, New York.

Nguyen, H. V., and C. Caloz (2007), Anisotropic backward-wave metasubstrate and its application to a microstrip leaky-wave antenna, paper presented at CNC/USNC National Radio Sci. Meeting, Union Radio Sci. Int., Ottawa.

Oliner, A. A., and D. R. Jackson (2007), Leaky-wave antennas, in *Antenna Engineering Handbook*, 4th ed., edited by J. L. Volakis, chap. 11, pp. 11-1–11-55, McGraw-Hill, New York.

Pendry, J. B., A. J. Holden, D. J. Robbins, and W. J. Stewart (1999), Magnetism from conductors and enhanced nonlinear phenomena, *IEEE Trans. Microwave Theory Tech.*, *47*(11), 2075–2084.

Rotman, W., and N. Karas (1957), The sandwich wire antenna: A new type of microwave line source radiator, *IRE Int. Conv. Rec.*, *5*, 166–172.

Sievenpiper, D., L. Zhang, R. F. J. Broas, N. G. Alexopolous, and E. Yablonovitch (1999), High-impedance electromagnetic surfaces with a forbidden frequency band, *IEEE Trans. Microwave Theory Tech.*, *47*(11), 2059–2074.

Trentini, G. V. (1956), Partially reflecting sheet arrays, *IRE Trans. Antennas Propag.*, *4*(4), 666–671.

Tretyakov, S. A. (2003), *Analytical Modeling in Applied Electromagnetics*, Artech House, Norwood, Mass.

Yakovlev, A. B., M. G. Silveirinha, O. Luukkonen, C. R. Simovskiand, I. S. Nefedov, and S. A. Tretyakov (2009), Characterization of the surface-waves and leaky-waves propagation on wire medium slab and mushroom

structures based on local and nonlocal homogenization models, *IEEE Trans. Microwave Theory Tech.*, *57*(11), 2700–2714.

Zhao, T., D. R. Jackson, J. T. Williams, H.-Y. D. Yang, and A. A. Oliner (2005), 2-D periodic leaky-wave antenna—Part I: Metal patch design, *IEEE Trans. Antennas Propag.*, *53*(11), 3505–3514.

A. Alvarez-Melcon, Department of Information and Communication Technologies, Technical University of Cartagena, E-30202 Cartagena, Spain.

C. Caloz and A. Shahvarpour, Poly Grames Research Center, Department of Electrical Engineering, École Polytechnique de Montréal, Centre de Recherche en Électronique Radiofréquence, 2500, ch. de Polytechnique, Montréal, QC H3T 1J4, Canada. (attieh.shahvarpour@polymtl.ca)